Achieving Ambient Stability and Suppressing Spin-Phonon Coupling in Dyprosocenium SIMs via MOF Encapsulation

Reshma Jose [a] †, Garima Bangar [a] †, Rajanikanta Rana[a], and Gopalan Rajaraman *[a]

[a] Department of Chemistry, Indian Institute of Technology Bombay, Powai, Mumbai400076, India. Tel: (+91)-22-2576-7183. Email: rajaraman@chem.iitb.ac.in

† Authors have contributed equally

Abstract:

Detailed ab initio CASSCF calculations coupled with periodic DFT studies on $[(Cp^*)Dy(Cp^{iPr5})]^+$ molecule encapsulated in a metal-organic framework found that MOF encapsulation offers stability to these fragile molecules keeping intact the Ueff values. Most importantly, this encapsulation suppresses the key vibrations responsible for reducing the blocking temperature offering a hitherto unknown strategy for a new generation of SIM-based devices.

Single-molecule magnets (SMMs) are a class of molecules that retain magnetisation alike permanent magnets below blocking temperature (T_B).[1] They have garnered wide interest in the last decades due to their molecular-level information storage features, which offer potential applications in the fields of compact data storage, quantum computing, magnetic refrigeration, molecular spintronics, etc.[2] As very large T_B values are key to achieving the proposed compact data-storage application based on SMMs, there has been a concentrated effort over the last 10 years to improve the T_B value from liquid Helium to liquid nitrogen temperatures [3, 4]. While this has been accomplished via a trial-and-error approach, the dysprosium-metallocene class of molecule is considered an important milestone as it raised the T_B significantly compared to other classes of compounds. Various chemical strategies have been evolved to improve the T_B above liquid-nitrogen temperatures using dysprosium SIMs and this includes (i) $[Dy(Cp^{ttt})_2]^+$ (Cp^{ttt}=1,2,4-tri(tertbutyl) cyclopentadiene) showing U_{eff} value of 1277 cm^{-1} and a T_B of 60 K [5](ii) $[(Cp^{iPr4R})_2Dy]^+$ {R=Et, Me and Cp^{iPr4R} = 1,2,3,4-tetra(iso-propyl)-5-alkyl cyclopentadienyl} with U_{eff} value of 1380 cm^{-1} and a T_B of 66 K when R=Et and U_{eff} value of 1468 cm^{-1} and a T_B of 62 K when R=Me [6] (iii) $[(Cp^*)Dy(Cp^{iPr5})]^+$ (Cp^{iPr5} =penta-iso-propylcyclopentadienyl, Cp^* = pentamethylcyclopentadienyl) with U_{eff} value of 1541 cm^{-1} and T_B = 80 K [4], exceeding the threshold of liquid nitrogen was synthesized, providing better linearity in the $Cp_{centroid}$–Dy–$Cp_{centroid}$ angles along with shorter Dy–C_{Cp} bonds. Enhancing the T_B value further is one of the goals in this area, and at the same time, to realise the potential application proposed, it is important to obtain molecules that are stable under ambient conditions – all the molecules (i) to (iii) mentioned are unstable. Several extensive experimental and theoretical studies suggest the role of enhancing the crystal field splitting, improving the linearity of $Cp_{centroid}$–Dy–$Cp_{centroid}$ angles and controlling molecular vibrations by shifting them to be in off-resonance with electronic excitation are shown to enhance the T_B values.[7, 8] In this regard, we have explored the possibility of stabilising this class of molecules inside a suitable metal-organic framework using a combination of DFT and *ab initio* calculations (periodic DFT with PBE functional employing Cp2k suite[9] and CASSCF/RASSI-SO/SINGLE_ANISO using MOLCAS [10], spin-phonon relaxation was computed using the G09 suite; see computational details). Our aim is to not only obtain a suitable host but also explore the variation in the electronic/vibrational features of the molecule to seek higher T_B values upon

encapsulation. Metal–organic frameworks (MOFs) are an emerging class of porous materials built with the assembly of inorganic nodes and organic linkers to produce porous architectures.[11, 12] The peculiar properties of MOFs, such as porosity, surface area, and chemical functionality, allow the tailoring of the MOF structure to complement the properties of the encapsulated unstable materials. There are several experimental precedents wherein SMMs, such as Mn_{12}, are stabilized inside a MOF, leading to better SMM characteristics [13]. Also, there are examples where unstable/non-isolable molecules are stabilized if a suitable MOF topology is offered.[14-17] Inspired by these studies, we have explored the possibility of stabilizing [(*Cp**)Dy(*Cp*^{iPr5})] (**1**)[4] in a suitable MOF. An ideally suitable MOF should be (i) diamagnetic, (ii) pore size should be suitable to enable stability, (iii) MOF should be robust with permanent porosity and stable upon encapsulation, and (iv) suitable ligand framework, preferably aromatic linkers, so that **1** can be stabilized by non-covalent interactions.

To find the most suitable MOF, which fits the criteria (i)-(iv). We used the QMOF Database[18], as the QMOF database has 22,375 MOFs, we applied filters in the structural properties according to complex **1**. As the length of **1** is 7.6 Å. We gave a suitable range for pore-limiting diameter (6.5 to 8 Å) and largest cavity diameter (12.5 to 14.6). The limiting value of 14.6 Å was given for the largest cavity diameter considering a length of **1** plus additional space up to 3.5 Å each side for C–H•••π interactions. 65 MOFs came after this filter. We wanted to have a diamagnetic MOF to avoid interference in the magnetic properties of **1**. So, keeping all these things in mind. We found eight MOFs, and stable host-guest interactions were found only for two of the MOFs (See ESI Table **S1**), and only one of the MOF (MOF-5) was found to offer an

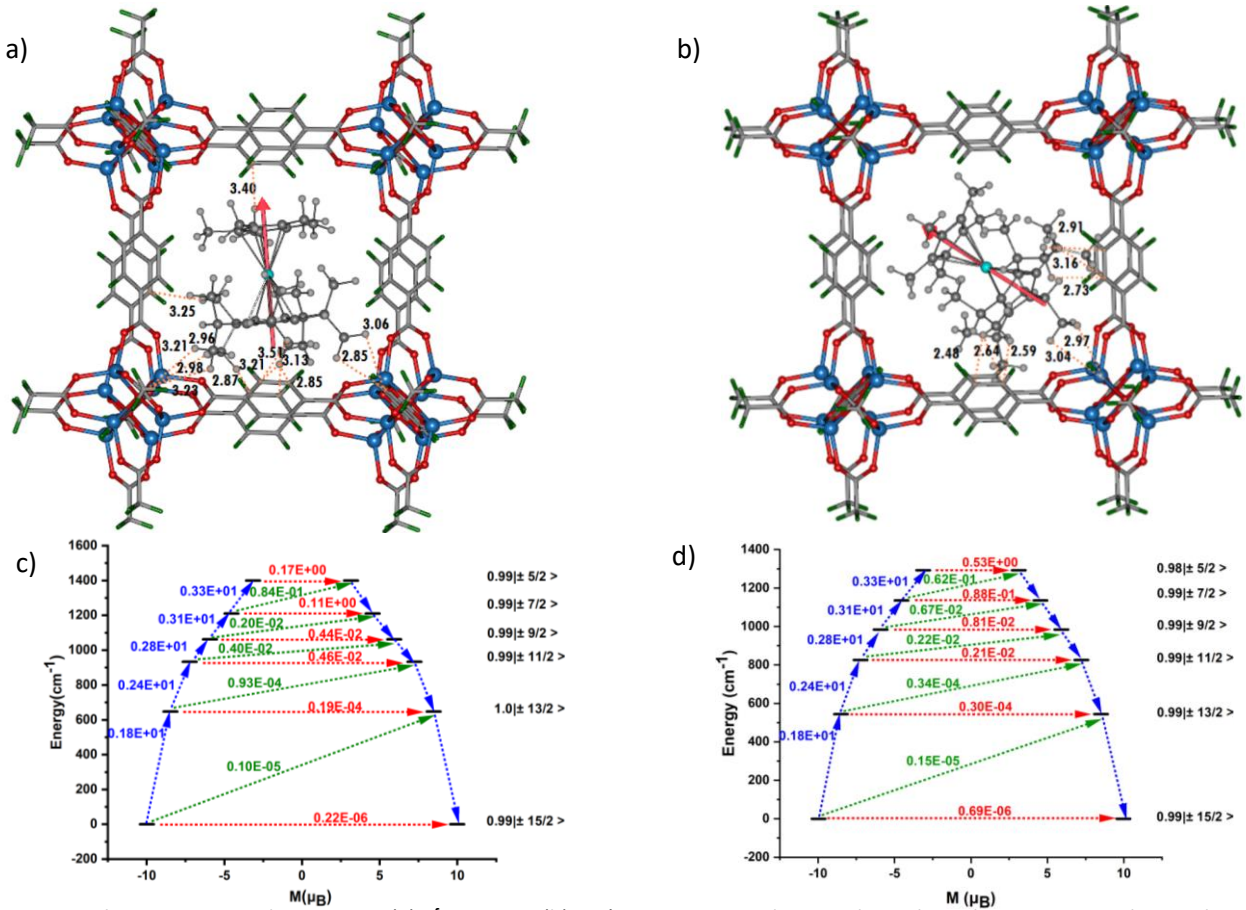

Figure 1. The DFT optimized structures: (a) **1**^{face}@MOF, (b) **1**^{vertex}@MOF. Dotted orange lines show the C–H•••π. Colour code: Dy(III) – Cyan blue, C – grey, O- red, and Zn-blue. The red arrow shows the ground state g_z axis. (c) and (d) shows *ab initio* computed magnetisation blockade barriers, along with computed transversal magnetic moments between the connecting pairs for complexes **1**^{face}@MOF and **1**^{vertex}@MOF respectively.

easier entry point while the other (Cd-BTT) not allow the **1** to enter. Thus, we narrow down the search to one experimentally synthesizable MOF, MOF-5 ($Zn_4O(BDC)_3$ (BDC= Benzene Di carboxylic acid) fulfilling all the criteria. The optimized geometries of **1** and MOF-5 are in agreement with the X-ray structure reported (Table **S3**). Further CASSCF calculations were performed on **1** for both X-ray and optimized structures using MOLCAS 8.2.[19] The U_{cal} values obtained for X-ray and optimized structures were 1390.9 cm^{-1} and 1399.6 cm^{-1}, respectively (Figure **S4**), showing close similarity. For our calculations, we have chosen a truncated model of MOF-5 (see Figure **S2b**). To determine the most stable conformation of **1** inside MOF-5, we optimized different orientations or conformers of **1** inside MOF-5 (Figure **1** and **S5**) (**1**^{edge}@MOF, **1**^{face}@MOF, and **1**^{vertex}@MOF, where **1**^{edge}@MOF is in which *Cp* ring is facing the edge of the cubic unit cell i.e. linker moiety, **1**^{face}@MOF is in which *Cp* ring is facing the face of the cubic unit cell i.e. void space, and **1**^{vertex}@MOF is in which *Cp* ring is facing the edge of the cubic unit cell i.e. nodes of the MOF. The computed binding energy (BE) for **1**^{face}@MOF (–215.6 kJ/mol) was higher compared to other orientations (see Table **S5** for BE details). Also, the *Cp*–Dy–*Cp* angle was comparatively slightly more linear (161.2°) in **1**^{face}@MOF, whereas slight bending of *Cp*-Dy-*Cp* angle was witnessed in **1**^{edge}@MOFand **1**^{vertex}@MOF. Further, to investigate the stability of various orientations, we have computed the possible C–H•••π interactions (in the range of 2.0–3.5 Å) in the system (Table **S7**). There exist ~19 strong MOF-5 for **1**^{face}@MOF, followed by 14 for **1**^{vertex}@MOF and 11 for **1**^{edge}@MOF, reaffirming the stability of *Cp**/*Cp*^{ipr5} ring and π cloud of benzene linker of order of the orientations. C–H•••π interactions among C-H bonds

Further to reaffirm the stability of the species inside MOF, molecular migration of (**1**^{face}@MOF) inside MOF-5, was checked by displacing the **1** from the equilibrium geometry 3 Å per step until the molecule comes out from MOF-5. In the realm of materials science, Metal-Organic Frameworks (MOFs) represent intricate extended structures characterized by the recurrence of unit cells in three-dimensional space. In the present study, we investigate the behavior of MOFs under the influence of complex **1**, subjecting them to controlled bombardment. We noticed the energy of **1** is lower near the walls compared to the center of the MOF. Surprisingly, despite the energy disparities favoring the periphery, the MOF experiences a consistent external force exerted by neighboring instances of complex **1**. This persistent pressure compels the **1** to traverse towards the center of MOFs void space. Remarkably, stability is eventually achieved upon encapsulation, a phenomenon that instills confidence in the viability of the selected experimental configuration(Figure **S9**).

The **1**^{face}@MOF showed a highly anisotropic ground state (M_J=±15/2) with negligible transverse components (g_x=g_y=0.0 and g_z= 19.978) (Table **S6**), where g_z axis passes through Dy by piercing the *Cp* rings. In the six lowest doublets, the crystal field (CF) exhibits a highly axial nature, with each state predominantly associated (greater than 96% character) with a definite projection of the total angular momentum, M_J (see Table **S6**). As the energy increases, the transverse components of the g-tensors roughly escalate by an order of magnitude in each doublet. Notably, in the fifth doublet, the transverse components become non-negligible, and in the sixth doublet, they are substantial enough to permit significant tunnelling. In the two highest states, axiality weakens, leading to considerable mixing under the influence of the crystal field, likely influenced by the asymmetry of the coordination environment. The U_{cal} value for **1**^{face}@MOF is 1399.2 cm^{-1} (Figure **1c** and **S6**), while for **1**, the energy barrier for magnetisation reversal is computed for X-ray (optimized structure) were 1390.9 cm^{-1} (1399.6 cm^{-1}) and the magnetisation relaxation occurs via the 6th excited state only. This is suggesting that the encapsulation of **1** inside MOF is retaining the U_{cal} value and simultaneously providing better stability to **1**. To understand the encapsulation of **1** in more detail, we plotted the partial density of the state diagram (Figure **2a**, **S7**, and **S8**). The peaks corresponding to Zn are moving towards the valence band upon interacting with **1** which is indicating a stable charge transfer

interaction. The peaks corresponding to linker oxygen atoms are moving upon interaction with **1**, suggesting the existence of CH…O interaction with the oxygen of MOF and **1**. The shifting of carbon peaks more towards the valence band is validating the stable CH..π interactions among MOF and **1**. The presence of C and H peaks of *Cp** near the valence band is reiterating the favourable binding energy for **1** inside the MOF. Hence the pDOS plot is validating the favourable host-guest interaction and thereby changes in characteristics of the MOF.

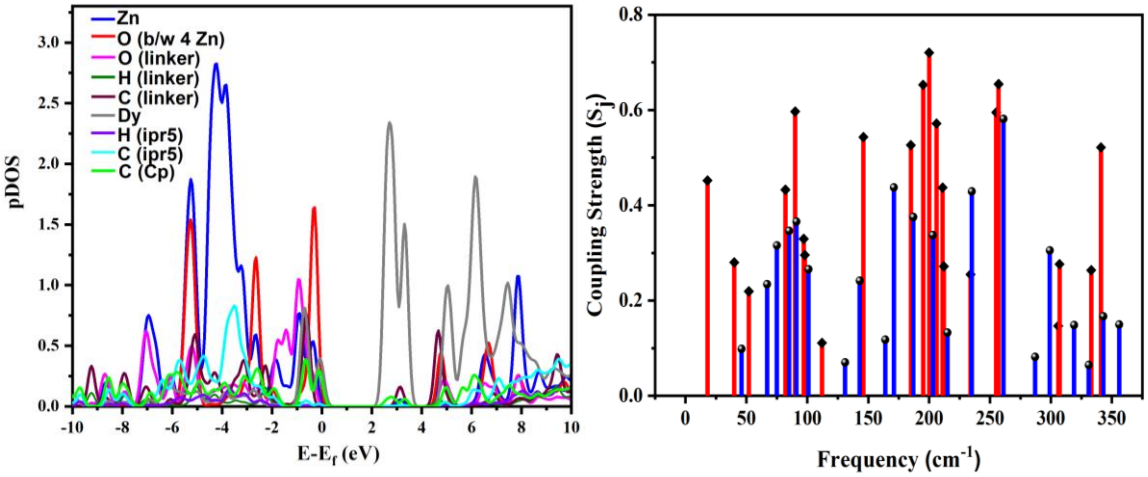

Figure 2. (a) Partial density of states plot for closest C-H•••π interaction and nearby atoms for **1**^{face}@MOF. (b) *Ab initio* calculated vibronic coupling strength (S_j) of the vibrational modes of **1** (red) and **1**^{face}@MOF (blue).

The critical property for characterizing any single-molecule magnet (SMM) is the blocking temperature (T_B). In our study, we observe the molecule getting stabilized upon encapsulation inside the MOF. The question arises: can this encapsulation effectively suppress spin-vibronic coupling, thereby enhancing the T_B? To address this, we aim to calculate the spin-vibronic coupling strength using Chilton's method.[21] As spin-vibration coupling plays a pivotal role in reducing the Blocking temperature of Single-Molecule Magnets (SMMs), quantifying this coupling is essential. To assess the spin-vibronic coupling, we employ CASSCF-SO calculations on distorted molecular geometries along each normal mode coordinate. The vibronic coupling coefficient $\left(\frac{\partial B_k^q}{\partial Q_j}\right)_{eq}$ is calculated, and we fit the change in CFP with a third-order polynomial (refer to Supporting Information). The overall vibronic coupling strength for each mode as S_j (refer to Eq. (1)).[20, 21] It is important to note that $B_{k,q}$ represents CFPs is expressed as linear combinations of the CFPs in Stevens notation B_k^q.

$$S_j = \sqrt{\frac{1}{3}\sum_k \frac{1}{2k+1}\sum_{q=-k}^{k}\left|\left(\frac{\partial B_{k,q}}{\partial Q_j}\right)_{eq}\right|^2} \qquad \text{---------- 1}$$

We calculated the principal vibrations, specifically those with a notable oscillator strength exceeding 0.1. Frequencies exhibiting an oscillator strength below 0.1 were excluded from our computations to mitigate computational costs. The pivotal vibrations are illustrated in Figure **S10**. The spin-vibronic coupling strength (S_j) signifies that a mode possesses substantial spin-vibronic coupling when its S_j value is high leading to strong spin-vibrational relaxation. A significant trend emerged when comparing S_j values in **1** and **1**^{face}@MOF: S_j values decreased within the MOF (Figure **2b**), implying a decrease in coupling strength. This decrease indicated **1**^{face}@MOF complex could exhibit larger relaxation time/T_B upon encapsulation. Furthermore, a distinct shift in vibrational frequencies was observed. In the crystal structure, the first peak occurred at approximately 18 cm^{-1}, while it shifted to around 46 cm^{-1} within the MOF. This shift suggested that MOF encapsulation induced a frequency shift could make the spin-phonon

relaxation off-resonance and enhance the T_B values as suggested elsewhere. [7] Furthermore, when the molecule is within the MOF, the detected coupling strength (S_j) is lower compared to the crystal structure. This implies that encapsulation leads to the suppression of undesired spin-phonon coupling. Remarkably, this frequency shift was consistent across all modes, indicating stabilization of the complex within the MOF and a frequency shift suggestive of an increase in the blocking temperature. With this temperature, magnetic transitions become significant.

To this end, we have proposed a way forward to solve multiple problems in achieving SIMs that can function at higher/room temperatures. The study unveiled how encapsulation within the MOF altered spin-phonon coupling, suppressed QTM, induced frequency shifts, and enhanced molecular stability, shedding light on potential applications in magnetic materials research.

Conflicts of interest

There is no conflict of interest to declare.

References

1. R. Sessoli, D. Gatteschi, A. Caneschi and M. Novak, *Nature*, 1993, **365**, 141-143.
2. L. Bogani and W. Wernsdorfer, *Nat. Mater.*, 2008, **7**, 179-186.
3. F.-S. Guo, M. He, G.-Z. Huang, S. R. Giblin, D. Billington, F. W. Heinemann, M.-L. Tong, A. Mansikkamaki and R. A. Layfield, *Inorg. Chem.*, 2022, **61**, 6017-6025.
4. F.-S. Guo, B. M. Day, Y.-C. Chen, M.-L. Tong, A. Mansikkamäki and R. A. Layfield, *Science*, 2018, **362**, 1400-1403.
5. C. A. Goodwin, F. Ortu, D. Reta, N. F. Chilton and D. P. Mills, *Nature*, 2017, **548**, 439-442.
6. K. R. McClain, C. A. Gould, K. Chakarawet, S. J. Teat, T. J. Groshens, J. R. Long and B. G. Harvey, *Chem. Sci.*, 2018, **9**, 8492-8503.
7. D. Reta, J. G. Kragskow and N. F. Chilton, *J. Am. Chem. Soc.*, 2021, **143**, 5943-5950.
8. R. Nabi, R. K. Tiwari and G. Rajaraman, *Chem. Comm.*, 2021, **57**, 11350-11353.
9. T. D. Kühne, M. Iannuzzi, M. Del Ben, V. V. Rybkin, P. Seewald, F. Stein, T. Laino, R. Z. Khaliullin, O. Schütt and F. Schiffmann, *J. Chem. Phys.*, 2020, **152**, 194103.
10. G. Karlström, R. Lindh, P.-Å. Malmqvist, B. O. Roos, U. Ryde, V. Veryazov, P.-O. Widmark, M. Cossi, B. Schimmelpfennig and P. Neogrady, *Comput. Mater. Sci.*, 2003, **28**, 222-239.
11. H. Li, M. Eddaoudi, M. O'Keeffe and O. M. Yaghi, *Nature*, 1999, **402**, 276-279.
12. H.-C. Zhou, J. R. Long and O. M. Yaghi, *Journal*, 2012, **112**, 673-674.
13. D. Aulakh, L. Liu, J. R. Varghese, H. Xie, T. Islamoglu, K. Duell, C.-W. Kung, C.-E. Hsiung, Y. Zhang and R. J. Drout, *J. Am. Chem. Soc.*, 2019, **141**, 2997-3005.
14. T. Zhang, K. Manna and W. Lin, *J. Am. Chem. Soc.*, 2016, **138**, 3241-3249.
15. F. Sha, Y. Chen, R. J. Drout, K. B. Idrees, X. Zhang and O. K. Farha, *iScience*, 2021, **24**, 102641.
16. K. K. Tanabe, N. A. Siladke, E. M. Broderick, T. Kobayashi, J. F. Goldston, M. H. Weston, O. K. Farha, J. T. Hupp, M. Pruski and E. A. Mader, *Chem. Sci.*, 2013, **4**, 2483-2489.
17. X. Xu, M. Ma, T. Sun, X. Zhao and L. Zhang, *Biosens.*, 2023, **13**, 435.
18. A. S. Rosen, S. M. Iyer, D. Ray, Z. Yao, A. Aspuru-Guzik, L. Gagliardi, J. M. Notestein and R. Q. Snurr, *Matter*, 2021, **4**, 1578-1597.
19. F. Aquilante, J. Autschbach, R. K. Carlson, L. F. Chibotaru, M. G. Delcey, L. De Vico, I. Fdez. Galván, N. Ferré, L. M. Frutos and L. Gagliardi, *Journal*, 2016.

20. A. Ullah, J. Cerdá, J. J. Baldovi, S. A. Varganov, J. Aragó and A. Gaita-Arino, *J. Phys. Chem. Lett.*, 2019, **10**, 7678-7683.
21. J. G. Kragskow, J. Marbey, C. D. Buch, J. Nehrkorn, M. Ozerov, S. Piligkos, S. Hill and N. F. Chilton, *Nat. Comm.*, 2022, **13**, 825.